Int J Thermophys (2009) 30:1938–1959
DOI 10.1007/s10765-009-0678-z

Abrupt Increase of the Absorption Coefficient of Alumina at Melting by Laser Radiation and Its Decrease at Solidification

Vadim A. Petrov

Received: 14 January 2009 / Accepted: 4 November 2009 / Published online: 25 November 2009

Abstract Experimental data for the normal-hemispherical reflectivity R of remolded aluminum oxide ceramics for wavelengths of (0.488, 0.6328, 1.15, and 3.39) μm and effective (radiance) temperatures T_{eff1} and T_{eff2} for wavelengths of 0.55 μm and 0.72 μm were obtained in the process of rapid subsecond heating by CO_2 laser radiation in air and vacuum from room temperature to the formation of thin molten layers of 0.6 mm to 0.7 mm thickness and of subsequent rapid free cooling with solidification of the melt when the laser radiation was blocked. Experimentally and by numerical simulation of combined radiation and conduction heat transfer, the influence of the heating radiation flux on the formation of the thin melt on the surface of ceramics with an abrupt increase of T_{eff1} and T_{eff2} and on the signal of the spectrometer in the infrared range from 2 μm to 11 μm at melting and on its decrease at solidification were studied. The radiation heat flux varied from 500 $\text{W} \cdot \text{cm}^{-2}$ to 2000 $\text{W} \cdot \text{cm}^{-2}$. It is shown that the determining effect on the temperature field and on the intensity of outgoing radiation is caused by the formation of the isothermal continuous two-phase zone and the abrupt increase (decrease) of the absorption coefficient of the melt. The importance of kinetics in the abrupt change of the absorption coefficient of molten Al_2O_3 is noted.

Keywords Absorption coefficient · Combined radiation and conduction heat transfer · Effective temperatures · Molten aluminum oxide · Rapid heating and cooling · Reflectivity · Semitransparent wavelength range

V. A. Petrov (✉)
Moscow State Institute of Radio Engineering, Electronics, and Automation (Technical University), 78, Prospekt Vernadskogo, Moscow 119454, Russia
e-mail: vapetrov@mirea.ru

1 Introduction

The wavelength and temperature dependencies of the absorption coefficient α of a single crystal of aluminum oxide (leucosapphire) in the main part of the semitransparent region are known quite well. The discrepancies of results in the wavelength range from 3.5 μm to 6 μm, obtained by various authors, are comparatively small. There are not enough data in the range from 1 μm to 3 μm at high temperatures. The analysis of the experimental data obtained before 1982 and the recommended values of α in the spectral range from 0.5 μm to 7 μm and in the temperature range from 300 K to 2300 K, i.e., almost to the melting temperature (2327 K), is presented in [1]. After that, new data on the absorption coefficient of the Al_2O_3 single crystal at high temperatures were not published; although, the question about changes of the thermal radiative properties in the pre-melting temperature range was discussed actively [2–6]. Small-scale plots of the dependence of the emissivity ε on wavelength λ are presented in [2,3]. Only in [4], the scale of the $\varepsilon(\lambda)$ plot allows estimation of the value of the absorption coefficient of the Al_2O_3 crystal near the melting temperature.

Apparently, the discontinuous increase of the absorption coefficient at the transition of the Al_2O_3 from the solid-to-liquid state was noted first in [7]. Indeed, direct measurements of α of the Al_2O_3 melt in that study were not carried out, but the significant difference of the radiance temperature of the crystal and the melt near the edge of the pool, generated by fusing the central part of the single crystal sample, was discovered. From the estimation made in that study, it was reported that α of a melt at the wavelength of 0.65 μm is 30 to 40 times more than α of a crystal near the melting temperature. After solidification, an irreversible change of α as compared with the initial crystal was not observed.

The bulk of the results of later direct or indirect investigations of α of the Al_2O_3 melt that are available in the literature shows that its value in the semitransparent region is tens, hundreds, or thousands times that for the crystal in the vicinity of the melting temperature. This is demonstrated very clearly in the visible region by differences in the brightness of a half-melted suspended droplet or filament in a steady-state condition [8–10]. So it may be assumed that there is a discontinuous change of the absorption coefficient as the aluminum oxide passes from the solid-state into the molten-state through its melting temperature and vice versa. At the same time, the discrepancy of various data for the absorption coefficient of the Al_2O_3 melt, which can reach two or more orders of magnitude, is determined. Up to now, it is still not clear how α varies in the process of melting (solidification) and what is the reason for very large differences between the absorption of solid and liquid alumina.

However, it must be noted that not all researchers who studied the absorption coefficient of liquid alumina agree with its jump at melting and solidification [11–14]. In those studies, the optical properties of molten and solid alumina were determined by measuring the radiative emission or the transmission and reflection of Al_2O_3 particles in a flame or plasma torch. So the properties of solid particles were measured immediately after solidification. The obtained data were much higher than recommended [1] for the single crystal near the melting point. For example, according to Mularz and Yuen [11] at λ = 0.7 μm and $T = 2090$ K $\alpha = 34.1$ cm^{-1}, while at the same wavelength and $T = 2100$ K, according to Lingart et al. [1], $\alpha = 0.29$ cm^{-1}.

The authors of [11] and [12–14] explained this discrepancy by the distinction of the particle structure from the structure of a single crystal and the different amount of impurities. However, other explanations may be considered. For example, it may be supposed that droplets were not solidified completely, or there were errors in determination of the temperature, which was not measured directly but was determined using results of measurements of the flame temperature.

It must also be noted that the results for changes of the absorption coefficient at solidification should not be directly extended to melting. This difference was noted in [15]. It is the opinion of the authors of [15] that at the transition of Al_2O_3 from the solid-to-liquid state, the absorption coefficient increases jump-wise by several orders of magnitude, whereas at the inverse transition its smooth decrease continues for several hundred kelvin below the melting temperature. The reason for the latter behavior according to Anfimov et al. [15] and Plastinin et al. [16] lies in the fact that molten Al_2O_3 at rapid cooling crystallizes as the metastable γ phase, which on subsequent cooling transforms to the stable α phase. This transformation in the high-temperature excursion following recalescence was predicted for the first time apparently in [17]. However, there are many doubts on the reliability of this hypothesis. This hypothesis was based on thermodynamic analysis and kinetic considerations. For both of them, the thermodynamic properties of γ-Al_2O_3 (melting temperature, enthalpy, heat capacity, entropy of melting) published in [18] were used. However, these data are also hypothetical. As γ-Al_2O_3 is an unstable phase, experimental data on its enthalpy (and correspondingly its heat capacity) were obtained up to about 1200 K. At higher temperatures the data were calculated by means of extrapolation. So the calculation of the thermodynamic properties of γ-Al_2O_3 is conventional, and the use of the results of this calculation can lead to incorrect predictions.

Another problem is the effect of the gaseous environment on the optical properties of molten Al_2O_3. There are several studies of this problem [4,8,19,20]. It was shown that this effect can be significant, but discrepancies of the obtained results were considerable. It should be noted that the absorption coefficient of the melt in these studies was investigated at steady-state conditions.

Only a few papers are available in the literature on the rapid heating and melting of alumina. We are aware of three papers [21–23]. Noguchi and Kozuka [21] studied the process of heating and melting, and then cooling and crystallization in a solar furnace. Because of its small scale, no details may be distinguished in the photograph of a signal from an oscilloscope display, given as a result for Al_2O_3. Bober et al. [22] obtained data on the variation of the normal-hemispherical reflectivity $R_{0.63}$ for a wavelength of 0.63 μm under conditions of rapid heating of millisecond duration to a temperature of the order of 3900 K; they reported data on the spectral normal emissivity $\varepsilon_{0.63}$, which were calculated in accordance with Kirchhoff's law for non-transparent materials as $\varepsilon_{0.63} = 1 - R_{0.63}$. They used a very high flux density of heating radiation of about $10^5\ \mathrm{W \cdot cm^{-2}}$. As a result, the gradient of temperature at the surface was very high, and the heated layer was very thin. Therefore, no variation of $\varepsilon_{0.63}$ was observed up to the melting temperature. Bober et al. [22] obtained at the melting point a jump in emissivity of approximately 0.31 to 0.89, and this high level of $\varepsilon_{0.63}$ was retained up to 3900 K.

The paper of Kirillin et al. [23] deals with the procedure of measuring the melting temperature of refractory materials by laser heating. They give the results of measurement of the spectral ratio temperature for wavelengths of 0.685 μm and 0.885 μm as a function of time under conditions of heating of a sample of Al_2O_3 ceramics 1 mm thick by radiation of a CO_2 laser. At an instant of time corresponding to approximately 0.68 s from the beginning of heating, a local maximum of (2608 ± 20) K was observed for the time dependence of the spectral ratio temperature; this maximum was followed by a brief wave-like variation (approximately up to 0.7 s) which is associated with the process of melting by Kirillin et al. [23]; after that, a monotonic increase was observed. The reasons for such a variation were not analyzed in [23], and no explanation was given for the high value of the spectral ratio temperature corresponding to melting. Note that in the three studies mentioned above, alumina and its melt were not treated as semitransparent materials, the combined radiation and conduction heat transfer (RCHT) was not taken into account, and no analysis was made of the effect of the temperature field in the surface radiating layer on the intensity of outgoing radiation.

Thus, considering the various opinions on the character and the value of change of the absorption coefficient of Al_2O_3 at melting, it can be concluded that practically all researchers noticed its discontinuous increase after melting; although, the reason for this change and its dynamics are not elucidated up to now. This article is one more step in an attempt to understand this phenomenon.

2 Change of the Intensity of Radiation and the Spectral Reflectivity During Rapid Heating and the Following Free Cooling

In an effort to clear up the dynamics of change of the absorption coefficient of Al_2O_3 at melting and solidification, measurements of the normal-hemispherical reflectivity of the alumina ceramics in the process of its rapid heating by concentrated radiation of a CO_2 laser up to the formation of molten layers of different thicknesses on its surface and the following free cooling were carried out. The method of measurement was described in detail in [24]. It is based on the rapid measurement of radiation, reflected by the sample. Probing lasers of different wavelengths were used.

Two cycles of experiments were carried out. In the first, a CO_2 heating laser of 140 W with a sealed-off tube was used [25]. The heating spot diameter was about 3 mm to 3.5 mm. The diameter of the surface illuminated by the probing radiation was about 1 mm. A He–Ne laser of 0.6328 μm, 1.15 μm, and 3.39 μm wavelengths and an Ar laser of 0.488 μm wavelength were used for probing. The duration of heating in all the experiments was almost equal and amounted to approximately 2.25 s. The experiments were performed under heating the samples in ambient air at two flux densities, $q_1 = 1200\,\mathrm{W \cdot cm^{-2}}$ and $q_2 = 1600\,\mathrm{W \cdot cm^{-2}}$. The temperature of the sample was measured by registration of its outgoing radiation at wavelengths of 0.55 μm and 0.72 μm. In this case, the measured temperatures were the effective temperatures T_{eff1} and T_{eff2}. Those are the temperatures of a blackbody with outgoing intensities of radiation at these wavelengths equal to the measured intensities of radiation of a non-isothermal near-surface layer of the sample. Thus, the effective temperatures differ from the radiance temperatures which are applicable to opaque substances.

As the temperature is the most important parameter in determining the accuracy of the obtained results, a special high-speed pyrometer has been developed for its measurement. The first version of this instrument is described in [26]. Now considerable modifications of its electronic system have been carried out.

The pyrometer is operated as a two-channel monochromatic pyrometer with two interference filters (wavelengths of 0.55 μm and 0.72 μm, bandwidths of 80 nm and 50 nm) mounted in front of silicon photodiode detectors. The pyrometer has only the range from 1900 K to 4000 K due to the use of high precision logarithmic modules. The output voltage of these modules is proportional to the logarithm of dc signals determined by the radiances of the target. The pyrometer has a specially built front objective (combined silica glass and calcium fluoride lenses, focal length of 135 mm), which is designed to minimize spherical and chromatic aberrations in the range from 500 nm to 900 nm. The field of view is about 0.3 mm in diameter at a distance of 250 mm from the objective to the target. The temperature of the objective, detectors, beam splitter, amplifiers, and logarithmic modules is stabilized with an uncertainty of 0.05 K due to water cooling from an ultra-thermostat. The temporal response of the pyrometer was checked using a light-emitting diode under a square pulse source of the voltage. The rise time was less than 0.5 ms over the whole range of signals.

The output voltage U of the logarithmic modules with the use of Wien's approximation of blackbody radiation is related to the temperature by

$$U = A - B\frac{1}{T}. \tag{1}$$

This equation has been used for calibration of the pyrometer.

The pyrometer is calibrated by measurement of the radiation of a small hole of the tubular graphite blackbody model at the same geometrical conditions that takes place in the experiments. The temperature of the blackbody is controlled with a reference disappearing filament pyrometer EOP-66 that has a total calibration uncertainty of 4 K at 2300 K and 9 K at 3300 K. According to Eq. 1, a result of the pyrometer calibration is the linear dependencies of the signals U_1 and U_2 (in bits of analog-to-digital converter (ADC)) as functions of $(1/T)$ for both wavelengths. The typical standard deviations of the calibration points were usually less than 3 bit. It is propagated into a standard uncertainty of temperature equal to 5 K at 1900 K, 8 K at 2500 K, and 12 K at 3100 K.

For calculation of the total uncertainty of the measurement of the transient temperature during the experiments, it is necessary to take into account the uncertainties of the effective wavelengths, the calibration of the reference pyrometer, the calculated extinction of radiation in the glass window of the blackbody model at the calibration, the reliability of the blackbody model, the long-term stability of the pyrometer, the linearity of the detectors, and other factors. An evaluation of the various factors shows that the total uncertainty of the measured temperature is about 10 K at 1900 K, 14 K at 2500 K, and 23 K at 3100 K, which is equal to approximately two standard deviations for the linear calibration fit.

Given in Fig. 1, as an example, are the results of one experiment in which the normal-hemispherical reflectivity $R_{1.15}$ for a wavelength of 1.15 μm was measured in the process of heating with a smaller flux density q_1 as in the process of cooling after

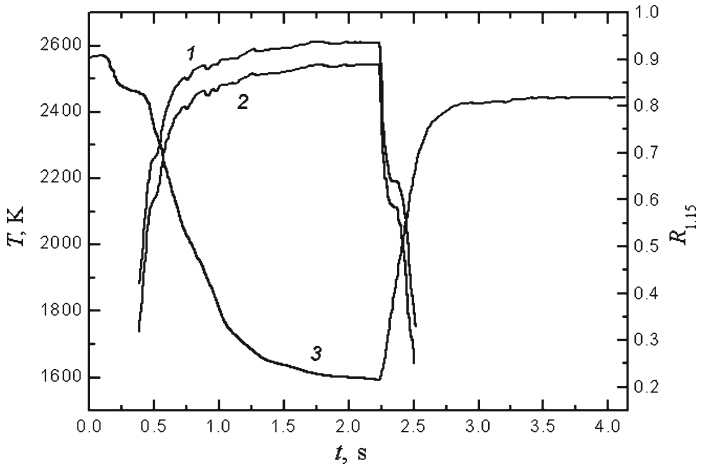

Fig. 1 Changes of the effective temperatures and the normal-hemispherical reflectivity in the process of heating with a flux density of 1200 W · cm^{-2} and subsequent cooling: *1*—T_{eff1}, *2*—T_{eff2}, and *3*— $R_{1.15}$

closing off the heating radiation with the shutter. The obtained time dependencies of $R_{0.48}$ and $R_{0.63}$ are similar in character to that of $R_{1.15}(t)$ at the same heating flux, as shown in Fig. 1. Figure 2 shows the averaged results for three series of measurements of $R_{0.48}$, $R_{0.63}$, and $R_{1.15}$ for heating with a flux density q_1. Each series consisted of five to eight quite reproducible experiments. These results are presented as the dependence of $R = f(T_{\text{eff1}})$. The numerated regions correspond to the heating stage; the cooling regions do not have the numerations. As can be seen from Fig. 2, for some time after the onset of functioning of the pyrometer, a region of a weak decrease of the reflectivity is observed. It takes place in the T_{eff1} range from 1900 K to 2200 K. At nearly 2260 K, a break of the $R = f(T_{\text{eff1}})$ dependence is observed; a short region with an increased speed of change of the reflectivity follows. After this short region of a steep decrease of R, a region with a monotonic decrease of R with a gradually increasing rate is seen in Fig. 2. As the temperature approaches a quasi-steady value, the rate of decreasing R slows slightly. On reaching the T_{eff1} quasi-steady-state value, $R_{1.15}$ and $R_{0.63}$ slightly decrease with continued heating along with an increase of the thickness of the melt up to its completion. $R_{0.48}$ reaches a quasi-steady-state value when a quasi-steady-state temperature is reached.

After shutting down the heating, the reflectivities $R_{1.15}$ and $R_{0.63}$ begin to increase considerably, although at a smaller rate, while there is a region at a constant value at the beginning of cooling for the dependence $R_{0.48}(T_{\text{eff1}})$. On cooling, the abrupt increase of the reflectivity at all the three wavelengths takes place near $T_{\text{eff1}} \approx 2200$ K. A continuous region with a gradual, monotonic increase of the reflectivity follows.

For heating with a larger flux density q_2 for the same time duration, the obtained results were somewhat different from that described above. At the larger flux density, the maximum value of the temperature T_{eff1} at the instant when the heating radiation is shut down is higher (about 2837 K in comparison with 2609 K), and the value of $R_{1.15}$, for example, is smaller (about 0.13 in comparison with 0.217). A break of the

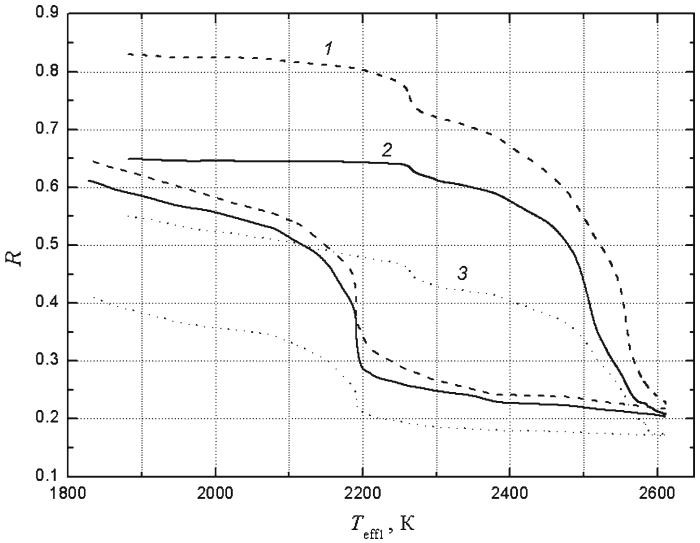

Fig. 2 Dependence of the normal-hemispherical reflectivity on the effective temperature T_{eff1} for heating with a flux density of $1200\,\text{W}\cdot\text{cm}^{-2}$ and subsequent cooling: *1*—$R_{1.15}$, *2*—$R_{0.63}$, and *3*—$R_{0.48}$

$R = f(T_{\text{eff1}})$ curve is observed at a higher temperature $T_{\text{eff1}} \approx 2380\,\text{K}$. It is essentially weaker than for heating with q_1. An increase of the reflectivity on cooling is not observed immediately after the heating radiation is shut down; it takes place some time later but before the temperature stops changing, connected with the solidification of the melt.

Here it must be noted that the obtained short region of the increased speed of drop of the reflectivity for the $R(t)$ dependence and the break for the dependence of $T_{\text{eff}}(t)$ during heating often do not correspond with the melting temperature, but take place at different effective temperatures. For quicker heating with a higher radiation flux density, the effective temperatures can be much higher than the melting temperature.

For heating in vacuum, the short region of the increased speed of change of the reflectivity for the $R(t)$ dependence and the break for the dependence of $T_{\text{eff}}(t)$ also take place; however, due to the higher value of the absorption coefficient of Al_2O_3 on heating in vacuum, the values of R and T_{eff} differ from those obtained in air.

In the first cycle of experiments, briefly described above, it was difficult to obtain a one-dimensional heat transfer and temperature field on the pyrometer sighting area of 1 mm in diameter. In view of this, other experiments (second cycle) were carried out, using a laser with a power of up to 1.2 kW for heating, which made it possible to increase the heating spot diameter up to 10 mm. Two series of experimental investigations were performed using different measurement procedures. In the first series, remolded alumina samples in a crucible with alumina powder were heated. High purity samples of Al_2O_3 were prepared by the repeated addition of powder, and they were melted using the concentrated radiation of a CO_2 laser. Thus, the samples were low scattering Al_2O_3 high-density polycrystals. In this case, comparisons of the experimental results with the results described below, obtained by numerical simulation, may be attained. Figure 3 is a schematic diagram which shows the experi-

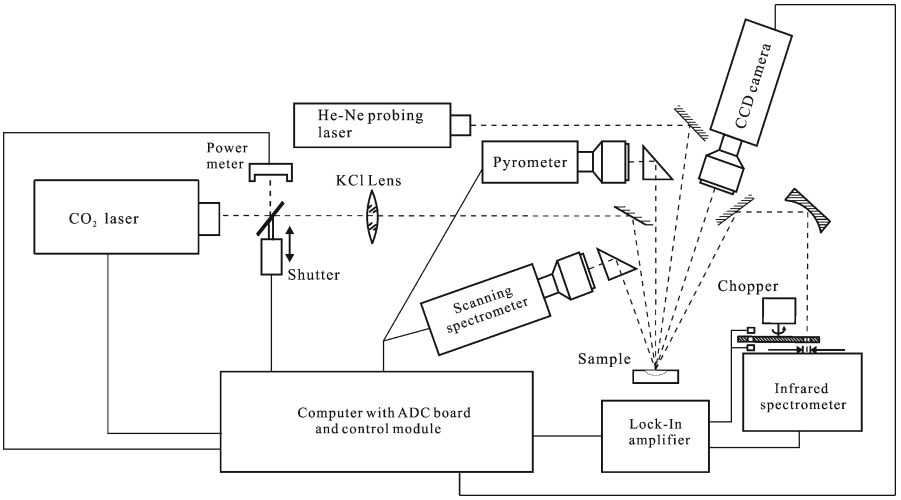

Fig. 3 Schematic diagram of experimental setup

mental arrangement in this series. Two effective temperatures T_{eff1} and T_{eff2} were measured by the pyrometer. The high-speed scanning spectrometer measured the effective temperatures in the spectral range from 0.5 μm to 1.5 μm in a quasi-steady state before cooling.

The infrared spectrometer measured a signal at one wavelength in the range from 2 μm to 10 μm. Because of the impossibility of ensuring complete identity of the external optics for calibration and measurements, this spectrometer was not calibrated against blackbody radiation. Therefore, the effective temperature in the IR range could be calculated only in the region of strong absorption, where the surface radiance temperature T_{r} was in fact measured. In so doing, the reference point was provided by the true temperature at the beginning of the solidification plateau after supercooling or at the respective kink in the thermogram. This temperature was taken to be 2327 K [18]. Given in Fig. 4, by way of example, is the result of one experiment in which the spectrometer registered the radiation at the wavelength of 8 μm in the region of high absorption [27]. The heating time was 12 s, with a flux density of heating laser radiation of 900 $\text{W} \cdot \text{cm}^{-2}$. One can see that, at approximately 1.3 s from the beginning of heating, the increase in the effective temperatures measured by the pyrometer is arrested; for the next 0.4 s, they are observed first to decrease and then to increase smoothly; at the instant of time corresponding to approximately 1.7 s, a steep rise of T_{eff1} and T_{eff2} and of the radiance temperature $T_{\text{r}(8\,\mu\text{m})}$ for the wavelength of 8 μm occurs. Note the fact that, at the instant when the increase stops (1.3 s), the effective temperatures T_{eff1} and T_{eff2} are appreciably lower than the respective effective temperatures on the solidification plateau (in the range of 12.4 s to 12.7 s), and the values of the radiance temperature for 8 μm at these intervals of time are approximately the same. Note further that the duration of the solidification plateau for $T_{\text{r}(8\,\mu\text{m})}$ is longer than that for T_{eff1} and T_{eff2}.

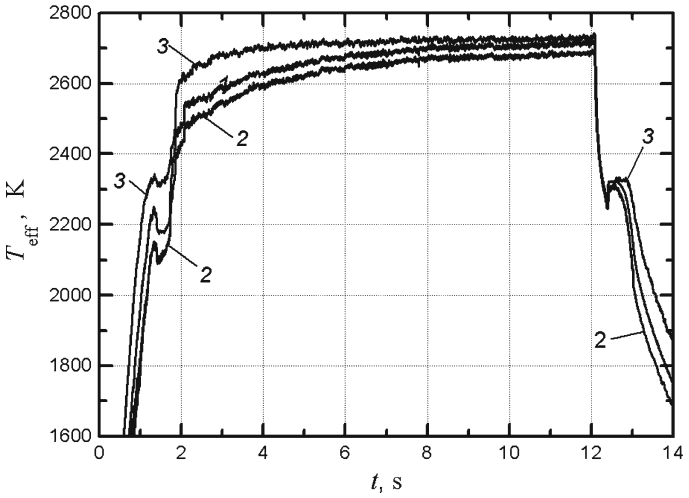

Fig. 4 Changes of the effective temperatures in the process of heating with a flux density of 900 $W \cdot cm^{-2}$ and subsequent cooling: *1*—T_{eff1}, *2*—T_{eff2}, and *3*—$T_{eff\,(8\,\mu m)}$

In the second series of experimental investigations, samples of Al_2O_3 ceramics were heated in an integrating sphere. The measurement procedure is described in detail in [24]. As previously, the measurement procedure was based on high-speed recording of radiation of probing lasers at the desired wavelength reflected from the sample being investigated under conditions of intense heating of the sample by radiation with a continuous CO_2 laser with a wavelength of 10.6 μm. The heating spot diameter ranged from 8 mm to 10 mm. A helium–neon laser (wavelength of 0.6328 μm) and an argon laser (wavelength of 0.514 μm) were used as probing lasers. The probing radiation was directed onto the sample center at an angle of 10° to the normal; this enabled one to assume the incident radiation to be normal to the surface. The diameter of the illuminated area was about 1 mm. The sample under investigation was placed at the center of the integrating sphere, and its reflection was compared to that of the reference at room temperature. The experiments were performed under conditions of heating the samples in ambient air. Samples of grainy ceramics in the form of disks, 45 mm in diameter and 6 mm to 8 mm thick, were investigated. Other oxide impurities did not exceed 0.5 %. The porosity of the samples was about 25 %. For comparison of the obtained results with numerical simulation, the majority of the experiments involved the use of samples subjected to pre-heating, as a result of which a dense crystallized layer of melt is formed on the surface. A study of the structure of the fracture cross section of the sample after the experiments revealed that the thickness of this crystallized layer was 600 μm to 700 μm. The experiments differed in the duration of the heating of the samples and in the flux density of the heating radiation. Shown in Fig. 5 as an example are the results of an experiment in which the reflectivity $R_{0.51}$ was measured for a wavelength of 514 nm in the process of heating with a flux density $q = 1780\ W \cdot cm^{-2}$. It is a factor of two higher than the flux density in the experiment presented in Fig. 4. So the heating rate was also higher. A comparison of these figures

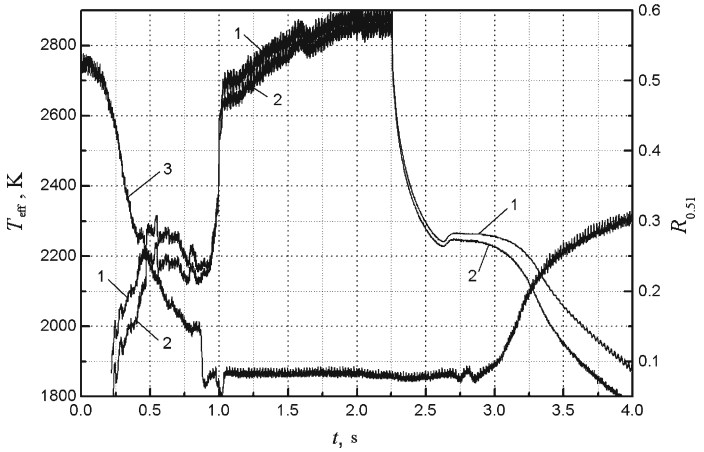

Fig. 5 Changes of the effective temperatures and the normal-hemispherical reflectivity in the process of heating with a flux density of 1780 W · cm^{-2} and subsequent cooling: *1*—T_{eff1}, *2*—T_{eff2}, and *3*—$R_{0.51}$

shows that at a greater heating rate the decrease of the effective temperatures at the initial stage of melting begins at higher values similar to the values for the solidification plateau where the thickness of the melt is larger. It means that at a greater heating rate the decrease of the effective temperatures begins when the surface temperature exceeds essentially the melting temperature.

It may be seen in Fig. 5 that at the instant of 0.94 s a sharp increase of the effective temperatures begins. For example, T_{eff1} increases from 2210 K to 2680 K. Of course, such an increase of the effective temperatures in this series of experiments, just as in previous ones, cannot be caused by an appropriate increase of the real temperature. It can be only due to an abrupt increase of the absorption coefficient for the wavelength of the measured outgoing radiation. In this case, the pyrometer abruptly begins to measure the radiation, outgoing from the thinner surface layer where the temperature is higher. Due to the abrupt increase of the absorption coefficient at the wavelength of 0.51 μm, the reflectivity $R_{0.51}$ abruptly decreases, the molten layer becomes optically infinite, and the value of the reflectivity is determined only by the surface of the melt.

In the second series of experiments, different heating fluxes were also used. Figure 6 shows the results for the smallest of them, $q = 515$ W · cm^{-2}. In this experiment, the heating time duration was larger and a lengthy temperature arrest was observed from 2.1 s to 3.65 s. The abrupt increase of the effective temperatures followed. T_{eff1} and T_{eff2} at the plateau were essentially larger than at solidification just after supercooling at the instant of 5.44 s. It means that a molten layer with its surface temperature above the melting point existed before the appearance of the plateau. At that, the thickness of the melt was less, even at the end of the plateau, than it was before solidification. The reflectivity at a wavelength of 0.51 μm at the instant near the end of the plateau, as can be seen in Fig. 6, abruptly decreased. A section of the small slope for the dependence of $R_{0.51}(t)$ preceded this decrease.

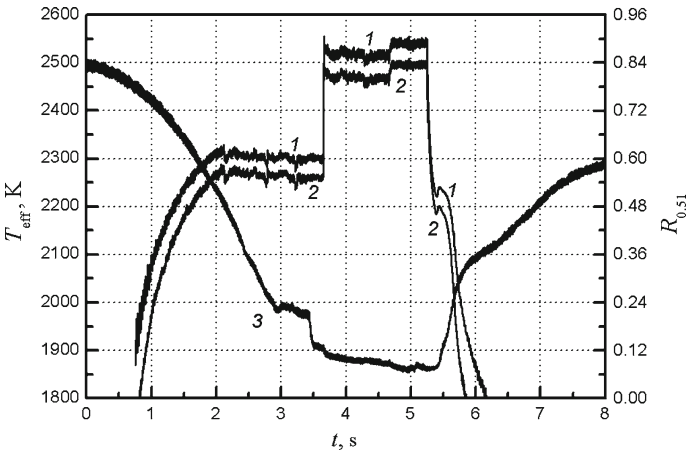

Fig. 6 Changes of the effective temperatures and the normal-hemispherical reflectivity in the process of heating with a flux density of 515 W · cm^{-2} and subsequent cooling: *1*—T_{eff1}, *2*—T_{eff2}, and *3*—$R_{0.51}$

This abrupt increase of the effective temperatures and decrease of the reflectivity, as in the experiments, shown in Figs. 4 and 5, cannot be explained by some reason except by an increase of the absorption coefficient.

To confirm the abrupt increase of the effective temperatures described above as a result of the increase of the absorption coefficient, computations of the temperature field were carried out.

3 Numerical Simulation of Al_2O_3 Heating by Concentrated Laser Radiation

The mathematical formulation of the problem of combined radiation and conduction heat transfer (RCHT) as applicable to the heating of semitransparent refractory oxides by concentrated laser radiation is given in [28]. In addition to the one-dimensional transient problem of RCHT, it takes into account the possibility of formation of a two-phase zone at melting and solidification, arbitrary non-linear boundary conditions for heat transfer at the front and rear surfaces of the sample, the dependence of the thermal properties of both the phases on temperature, and the dependence of the thermal radiation and optical properties on temperature and wavelength. Because of the absence of experimental data on the absorption coefficient of Al_2O_3 at a heating radiation wavelength of 10.6 μm, its value was taken to be independent of temperature and equal to 1000 cm^{-1} for both solid and molten phases. It was assumed that in the semitransparent wavelength region from 0.4 μm to 7 μm, the absorption coefficient undergoes a jump increase immediately upon reaching the melting temperature. Our mathematical model in no way included any special features associated with rapid heating, although as seen from the experimental results, such special features can be present.

The transient heating of a planar layer of single crystal alumina 5 mm thick with free surfaces was considered. The calculations revealed that the two-phase zone in the

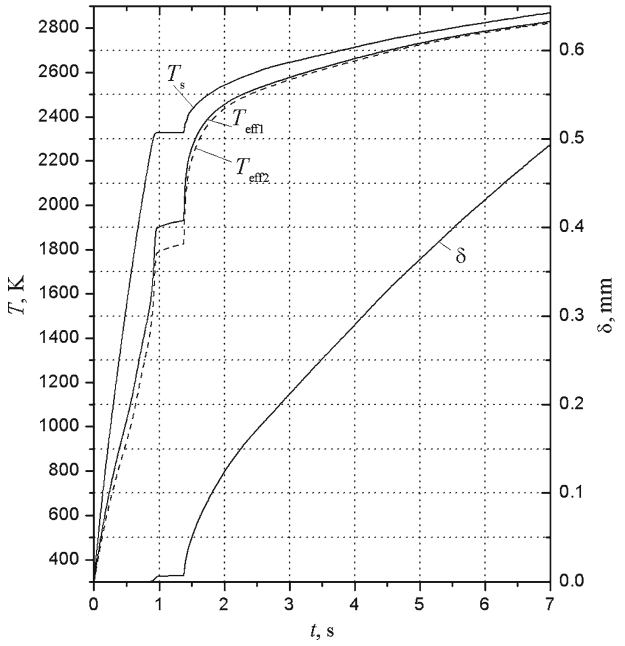

Fig. 7 Changes of the surface temperature T_s, effective temperatures T_{eff1} and T_{eff2}, and melt layer thickness δ under heating with a flux density of $600\,W \cdot cm^{-2}$

process of heating is very thin and forms only at the initial stage of melting. Figure 7 gives the results of calculation of the heating time dependence (at a heating flux density of $600\,W \cdot cm^{-2}$) of the surface temperature T_s, melt thickness δ, and effective temperatures T_{eff1} and T_{eff2} at wavelengths of 0.55 μm and 0.72 μm. The values of these wavelengths correspond to those of the pyrometer employed by us in the experimental investigations. One can see that, at the initial stage of melting, where the isothermal two-phase zone is present, the effective temperatures are much lower than the melting temperature. Figure 8 gives the analogous results obtained under heating with a flux density of $400\,W \cdot cm^{-2}$. In this case, the heating rate is lower, the melt thickness is much smaller at the same instants of time, and the two-phase zone also forms at the initial stage of melting and exists for a longer time than in the case of heating with a flux density of $600\,W \cdot cm^{-2}$. One can see that the maximum thickness of the isothermal two-phase zone in both the cases is approximately the same and less than 10 μm.

According to the computed results, another nature of a two-phase zone exists at solidification. Figure 9 shows, as an example, the computed results for temperature fields on cooling of the sample of 10 mm thick, which was heated by a CO_2 laser radiation flux of $600\,W \cdot cm^{-2}$ for 100 s. A section of 2-mm thickness from the heated surface is only shown. The first shown temperature distribution is concerned with the instant of 100 s, when the heating radiation was blocked. At this moment the thickness of the molten layer was equal to 0.625 mm. After 130 ms from the start of cooling, the surface temperature was reduced below the melting point temperature although

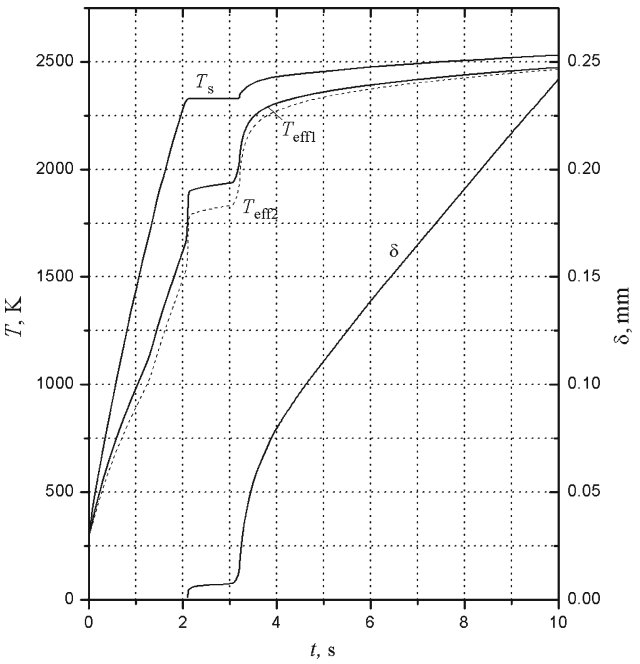

Fig. 8 Changes of the surface temperature T_s, effective temperatures T_{eff1} and T_{eff2}, and melt layer thickness δ under heating with a flux density of 400 W · cm^{-2}

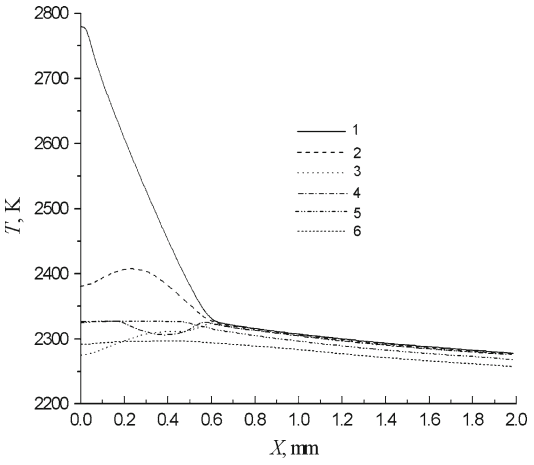

Fig. 9 Temperature distribution in surface layer at cooling and solidification at different instants of time: *1*—100 s, *2*–100.1 s, *3*–100.2 s, *4*–100.3 s, *5*–100.6 s, and *6*–100.8 s

a liquid state remained. The minimum surface temperature of the melt is about 50 K below the melting temperature. A two-phase zone appears near the surface after 0.2 s from the start of cooling. Its size increases very quickly. At 100.3 s, its thickness is equal to 180 μm; at 100.5 s, it is equal to 340 μm; and at 100.7 s, the two-phase zone occupies almost the whole layer which was in the molten state before cooling. It is significant that at the instant of 100.5 s a very thin solid layer appears at the

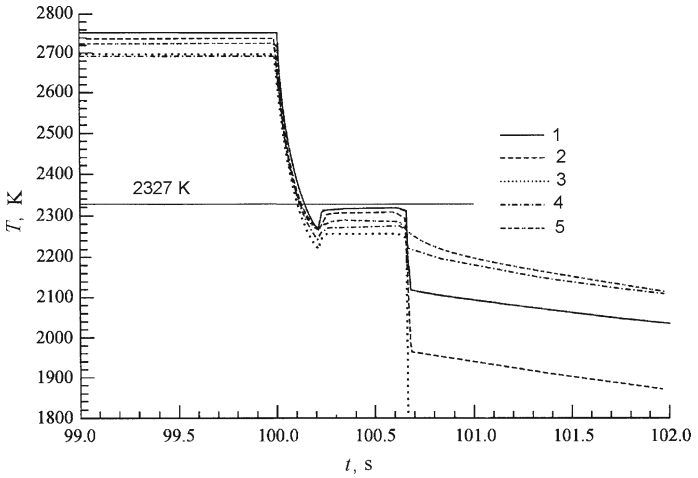

Fig. 10 Effective temperatures at cooling and solidification of thin layer: *1*—$\lambda = 0.5\,\mu$m, *2*—$\lambda = 1\,\mu$m, *3*—$\lambda = 2\,\mu$m, *4*—$\lambda = 5\,\mu$m, and *5*—$\lambda = 7\,\mu$m

surface, but its effect on the heat transfer is very small due to high transparency (low absorption). Its temperature is near the melting temperature. The process of complete solidification is sufficiently long, and it takes about 0.5 s. The calculated results for the time dependencies of the effective temperatures at different wavelengths during cooling and solidification are presented in Fig. 10. It is seen that after the end of the solidification plateau the effective temperatures decrease abruptly; the smaller is the absorption coefficient of a forming solid phase, the bigger is the jump of the effective temperature. As presented in Fig. 10, the smallest value of the absorption coefficient of the solid phase near the melting temperature occurs at a wavelength of 3 μm.

Examples of the experimental results for some effective temperatures during cooling and solidification of samples with the molten layer, for which the thickness was similar to that obtained from the calculated results, are presented in Figs. 4 and 5. It can be seen that at the end of solidification the effective temperatures for 0.55 μm, 0.72 μm, and 8.0 μm decrease quickly; however, the abrupt decrease, similar to the calculated result, is absent.

Typical scanning electron micrographs of the surface and fracture cross section of the solidified thin melt are presented in Fig. 11. The grain crystals of cubic-like shape and random orientation, which can be seen on the surface, confirm homogeneous nucleation and formation of a two-phase zone during solidification. X-ray analysis of the solidified melt showed the presence of only the α phase of the aluminum oxide.

4 Analysis of the Results

An analysis of the obtained results shows that at the beginning of melting, the rate of heating of the solid phase slows down, and the resultant very thin layer of the melt is optically transparent. The pattern of variation of effective temperatures in the melting region, as well as the melting process itself, depend significantly on the flux density.

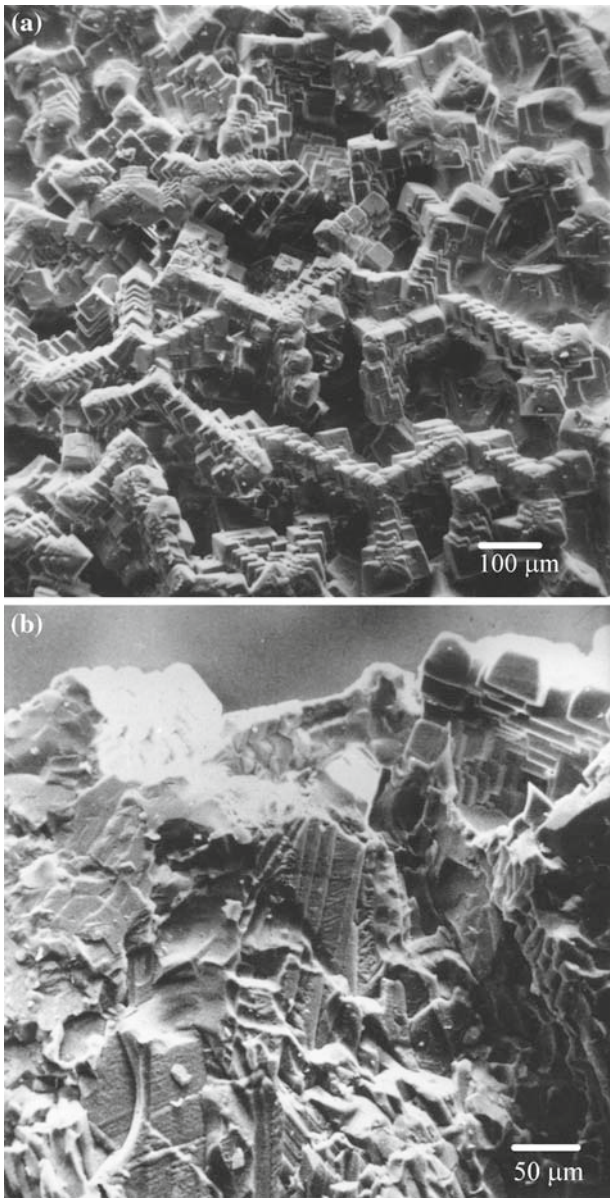

Fig. 11 Micrographs of (**a**) surface microstructure and (**b**) failure cross section of solidified layer

The results of numerical simulation of this process demonstrated (Figs. 7, 8) that the increase of the melt thickness has a very unequal rate. The first stage of melting is associated with the depth of penetration of the heating radiation of the CO_2 laser. Because it was assumed in the calculations that the absorption coefficient at a wavelength of 10.6 μm is 1000 cm^{-1}, this depth was approximately 10 μm. It follows from

Figs. 7 and 8 that an isothermal two-phase zone at a depth of slightly less than 10 μm is present at the beginning of melting. In so doing, the thickness of this two-phase zone is independent of the flux density; however, different times are required for its complete melting at different values of the flux density. Since this zone is very thin, the radiation leaving the layer in the semitransparent region is defined both by this isothermal two-phase zone and, to a significant degree, by deeper-lying colder layers of the crystal. Therefore, the effective temperatures in the interval of time during which the process of melting occurs in this zone are much lower than the melting temperature. For example, for a wavelength of 0.55 μm, the values of T_{eff1} at the instants of time of 0.97 s, 1.16 s, and 1.37 s (Fig. 7) are 1898 K, 1917 K, and 1931 K, respectively, and those at the instants of time of 2.16 s, 2.6 s, and 3.03 s (Fig. 8) are 1899 K, 1924 K, and 1936 K, respectively. Because the thickness of the two-phase zone is very small, the melt at this stage of heating must not affect the reflecting characteristics, as was confirmed by the experimental results. At this stage the energy input was largely spent for the heating of the solid phase under the thinnest layer of the melt. However, after some instant of time following complete melting of the two-phase zone, the energy input is largely expended into melting, and the melt thickness increases very rapidly. If a two-phase zone of less than 10 μm thickness melted during 0.4 s (Fig. 7), the thickness increased by 60 μm during only 0.2 s in the next stage.

The obtained experimental results correlate qualitatively with the calculated results for a number of special features of variations of measured characteristics. The small thickness of the melt layer at the initial stage of melting, which is defined by the depth of penetration of the heating radiation of the CO_2 laser, explains the experimentally observed deceleration of the rate of decrease in the reflectivity. An arrest of the effective temperatures T_{eff1} and T_{eff2} during melting was obtained in both the numerical simulation and the experiment measurements. But in the first case this zone of $T_{\text{eff}}(t)$ dependency was like a slightly inclined straight line (plateau), and in the second case, the line could have oscillations which changed into a short inclined straight line at a high flux density (Fig. 1) or into a horizontal plateau at a low flux density as is shown in Fig. 6.

For a better comparison of calculated results with experimental data, Fig. 12 gives the calculated values of T_{eff1} under conditions of heating an Al_2O_3 crystal 5-mm thick with three flux densities of 1200 $\text{W} \cdot \text{cm}^{-2}$, 600 $\text{W} \cdot \text{cm}^{-2}$, and 400 $\text{W} \cdot \text{cm}^{-2}$. These results are compared with the experimental results for remolded and solidified ceramics with a flux density of 515 $\text{W} \cdot \text{cm}^{-2}$, which was the minimal flux density in the entire investigated cycle. Because it was assumed in the mathematical model that α in the semitransparent region increases abruptly immediately at the instant when the melting temperature is reached, the calculation gives a step increase in the effective temperature before the beginning of the plateau caused by the high contribution from the surface layer radiation. The effective temperatures at the initial stage of melting during the formation of a two-phase zone are close and much lower than 2327 K because of the very small thickness of the two-phase layer and the determining contribution to outgoing radiation from the deeper layers.

In experiments with low values of the flux density, an extended plateau with $T_{\text{eff1}} \approx 2300$ K could be obtained; in so doing, the melt thickness increased and exceeded the calculated value of the two-phase zone. With the increasing flux density,

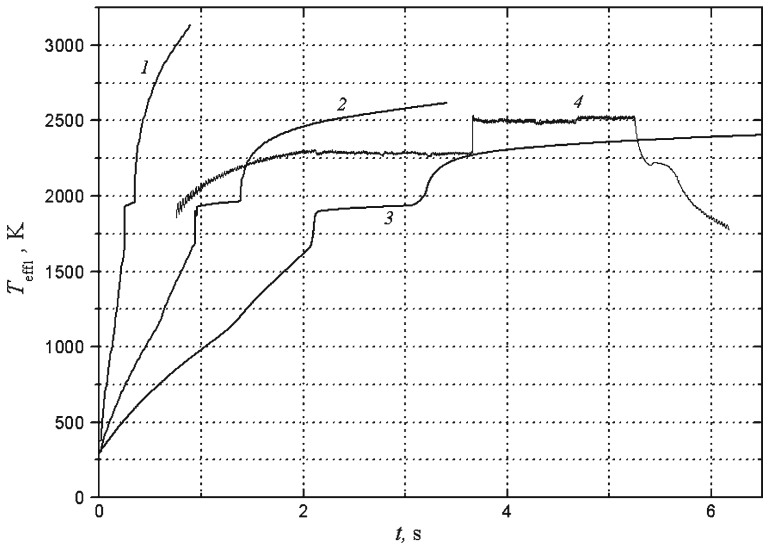

Fig. 12 Comparison of the results of calculation of T_{eff1} in the process of heating with the experimental results: *1*—$q = 1200\,\text{W}\cdot\text{cm}^{-2}$, *2*—$q = 600\,\text{W}\cdot\text{cm}^{-2}$, *3*—$q = 400\,\text{W}\cdot\text{cm}^{-2}$, and *4*—$q = 515\,\text{W}\cdot\text{cm}^{-2}$

the experimentally observed variation of the effective temperature in the initial region of melting reminded one of a wave consisting of a crest and a trough: the beginning of melting was expressed in the slowing down of the variation of T_{eff1} in the rising region of the wave, which was followed by a decrease in T_{eff1} after reaching a maximum. Sometimes, two periods of such waves were observed in the experiments. The reason for the oscillations of the $T_{\text{eff}}(t)$ dependence may be connected with an additional expenditure of energy in the melt. Note that if the heating by radiation was strictly surface heating, the melting front originating on the surface would gradually move deeper, the melt thickness would gradually grow, and no special features associated with the beginning of melting would be observed on the $T_{\text{eff}}(t)$ curves. At still higher values of flux density, the wave disappeared, and only a step existed similar to that shown by curve 1 in Figs. 1 and 12. It must be noted as a principal fact that, in all experiments, the halt in the variation of effective temperatures at the initial stage of melting was followed by their abrupt rise (jump).

Experiments with heating of the samples in a powder crucible revealed that a jump-like increase in effective temperatures occurs both in the semitransparent region and in the non-transparent region in which the absorption is defined mainly by atomic vibrations and is thereby associated with the short-range order of the relative arrangement of atoms of aluminum and oxygen in the melt. The abrupt increase in α of the melt may be caused by a variation of the coordination environment of Al atoms [29]. This variation will further cause an increase in α at the wavelength of heating radiation; given the high rate of this variation, this may cause an abrupt increase of the temperature field in the near-surface absorbing layer. In addition to the abrupt increase in α at $10.6\,\mu\text{m}$ and, thereby, the abrupt rise of temperature at the depth of penetration of the heating radiation, an additional increase in T_{eff1} and T_{eff2} is appar-

ently possible as a result of the abrupt increase in α at wavelengths of 0.55 μm and 0.72 μm. However, this is possible only if the real temperature decreases steeply from the surface deep into the melt. This may be very important at high heating fluxes and less important in experiments with a low flux density such as 515 $W \cdot cm^{-2}$. Our calculations revealed a less abrupt increase of the surface and effective temperatures because of the assumption that α at a wavelength of 10.6 μm is equal to 1000 cm^{-1} in both the solid and the liquid phases. The additional expenditure of energy for the atomic short-order transformation in the formed melt can lead to oscillations of the effective temperatures which were observed over a certain range of the heating flux.

As was mentioned above, the value of α of molten Al_2O_3 may be connected with the influence of the content and pressure of the surroundings, interactions with the container (if present), and the presence of admixtures in the initial samples of Al_2O_3. However, it is obvious that the main reason is in the properties of molten Al_2O_3 itself. It is known that the stable structure of a single crystal of pure Al_2O_3 is the α phase (corundum), which consists of close-packed planes of oxygen anions stacked in an hcp sequence with the Al cations occupying two thirds of the octahedral interstices between the anion layers. However, aluminum oxide has a series of metastable crystalline phases, which can be produced upon rapid solidification of micron and submicron droplets. In the most frequent cases, the γ phase is obtained, which has fcc oxygen packing characteristic of a spinel. It may be the indirect argument that, after melting of Al_2O_3, the local aluminum atomic order can differ from the lattice of corundum. It may be the reason for the non-monotonic change of the absorption coefficient. At the same time the process for formation of the different lattice structure on rapid solidification of the micron and submicron droplets remains unclear. In the most detailed study [17], it was obtained experimentally that solidified droplets of 0.01 μm to 0.1 μm in diameter are X-ray amorphous, the cubic spinel γ phase is the structure of solidified droplets between 0.1 μm and 10 μm in diameter, and the stable α phase structure takes place after solidification of droplets larger than 20 μm in diameter. However, according to the opinion of the authors of [17], the latter does not mean that the α phase is obtained immediately on solidification of the melt. They believed that it is very likely that the initial crystallization of the γ phase can be transformed into the α phase for the high-temperature excursion following recalescence. The experimental results for solidification, obtained in our study, do not show a very abrupt decrease of the effective temperatures, as was obtained in the calculations. But the decrease of the effective temperatures at the end of solidification was quite rapid, so it cannot be contended that this transformation from the α- to the γ-phase in the solid-state takes place.

For slow solidification, which take place in the growth of α-Al_2O_3 single crystals, there is a problem of capture of gas bubbles by a growing crystal from a melt. There are different points of view on the nature of this phenomenon. One of the causes of suspicion is the thermal dissociation of the melt [30]. According to Bagdasarov [30], a preferential evaporation of Al^{3+} ions can lead to violation of stoichiometry of the melt and to the capture of the gas products of dissociation at the front end of the crystallization. A violation of stoichiometry may be the reason for the higher value of the absorption coefficient of the melt in comparison with the crystal. However, it

seems more probable that the main reason is the change of the short-range order at melting. Lately several successful investigations were carried out in this direction. Among them, there are experimental studies [29,31–35] and molecular dynamics simulations [36,37]. Although there are some disagreements between various studies, most of them, except the results of [32], made the conclusion that the short-range order in molten alumina is defined essentially by a $(AlO_4)^{5-}$ basic unit, i.e., liquid Al_2O_3 exhibits γ-phase-like coordination. If such is the case, this may be the reason for the high value of the absorption coefficient of molten alumina. As was calculated in [38], the band gap for the γ phase of alumina at room temperature can be equal to 3.9 eV (in comparison to 8.8 eV for the α phase). So the melt may be considered as a semiconductor with a narrow band gap, especially at high temperatures, and it can have a large absorption coefficient over a broad wavelength range.

It should be noted that all experimental studies of the short-range atomic order in molten alumina were carried out at steady-state conditions, and the time duration for alumina being in the molten state amounted to minutes or tens of minutes. The transient process for the structural change has not been studied.

Considering the obtained results for Al_2O_3, it is very important to understand if the abrupt increase of the absorption coefficient at melting and its decrease at solidification is typical for other refractory oxides. This question has not been studied satisfactorily up to now. It may be assumed that this phenomenon can takes place if the refractory oxide changes atomic coordination at melting. Apparently, in addition to aluminum oxide, there are experimental data on the atomic coordination of melts for only yttrium oxide and aluminum–yttrium garnet [39] among the other refractory oxides. Based on these data, it may be surmised, that for these substances the discontinuous change of the absorption coefficient at melting and solidification can take place. However, it has not been confirmed experimentally up to now.

It may also be assumed that the jump of the absorption coefficient can take place if the refractory oxide has several crystal modifications and non-equilibrium structures can be formed on rapid cooling and solidification of the melt. In this connection it is obvious to consider zirconium oxide first. The study of cubic zirconia stabilized with yttria [40,41] revealed that a jump of the absorption coefficient was observed at melting and solidification at a wavelength of 0.63 μm (see Figs. 2, 6 in Ref. [40]) and at wavelengths of 0.488 μm, 0.63 μm, and 1.15 μm in Ref. [41]. The study of cubic zirconia stabilized with calcia [42] revealed that there is ample evidence of a significant change of absorption at melting and solidification, at least, at wavelengths of 1.15 μm and 3.39 μm. At the same time, explicit signs of a discontinuous change of the absorption coefficient of magnesium oxide were not observed [43]. It may be noted studies of the jump of the absorption coefficient at melting (solidification) of refractory oxides at a temperature of melting of about 3000 K is very difficult. The point is that a large number of free carriers is generated due to a reduction of the ratio of the band gap energy to the thermal energy, a reduction in the band gap, and formation of structural defects at these temperatures. It leads to a high value of the absorption coefficient over the broad wavelength range even in the solid state, and, consequently, it is very difficult to observe the jump of the absorption at the phase transition. Therefore, the question of the presence or absence of the jump of the absorption coefficient of various refractory oxides except for alumina and zirconia needs to be studied.

An aluminum oxide is the most convenient substance for studying the jump of the absorption coefficient, as it has a relatively low temperature of melting and a correspondingly low concentration of free carriers in the solid state near the melting point. It should be noted that only pure oxides are considered here, so any influence of admixture extrinsic charge carriers is neglected.

One addition to the status of knowledge on the jump of the absorption coefficient at melting of various oxides except alumina and zirconia should also be mentioned. It can be affirmed that our experiments on heating and melting by concentrated laser radiation of silica ceramics and silica glass resulted in the conclusion that a jump of the absorption coefficient of SiO_2 is not present.

5 Conclusions

It was observed that the jump of the absorption coefficient of Al_2O_3 takes place at melting and at solidification. The level of this jump is two orders of magnitude. For rapid heating, this jump does not occur at the instant of reaching the melting temperature. The temperature of this jump with laser heating can be higher than the melting point. Its value depends on the density of the heating radiation flux. The probable reason of the abrupt increase of the absorption coefficient may be a rearrangement of atoms in the melt and changes in the short-range atomic order. This increase is not instantaneous for the entire melt, and begins under certain conditions and continues for a certain, but very short period of time. This abrupt increase of the absorption coefficient at the wavelength of heating laser radiation of 10.6 μm causes a very fast abrupt increase of temperature in the surface layer, as is observed experimentally. The mathematical model of heating developed previously by us, which assumes that the absorption coefficient of alumina increases abruptly at the instant of reaching the melting temperature and decreases abruptly at solidification, fails to reflect the important part played by kinetics in the abrupt variation of the absorption coefficient in the melt. However, the kinetics of restructuring of the Al_2O_3 melt has scarcely been investigated to date. The published results of investigations of the short-range atomic order in the melt of Al_2O_3 were obtained at steady-state conditions. The abrupt change of the absorption coefficient at melting and solidification can be caused by changes of both the electronic structure and the short-range atomic order. An important contribution can also be attributed to the defects. The use of high-speed spectrometry over a broad wavelength range can help to understand the reasons and kinetics of the abrupt change of the absorption coefficient at melting under rapid heating and at solidification during high-speed cooling. It is a problem for further experimental study.

The other future problem concerns the developed mathematical model of heating and melting by concentrated laser radiation. It requires a correction to take into account the kinetics of the change of the absorption coefficient for a non-uniform temperature distribution in the surface layer.

Acknowledgments This study was supported by the Russian Foundation for Basic Research (Project No. 05-02-16290). The author thanks Drs. A. P. Chernyshev and A. Yu. Vorobyev for carrying out the experiments and Dr. V. E. Titov for development of computer codes for combined radiation and conduction heat transfer.

References

1. Yu.K. Lingart, V.A. Petrov, N.A. Tikhonova, Teplofiz. Vys. Temp. **20**, 872 (1982)
2. O. Rosenbaum, D. De Sousa Meneses, Y. Auger, S. Chermanne, P. Echegut, Rev. Sci. Instrum. **70**, 4020 (1999)
3. J.F. Brun, D. De Sousa Meneses, P. Echegut, in *Proceedings of the Fifteenth Symposium on Thermophysical Properties*, Boulder, Colorado, 2003
4. V. Sarou-Kanian, J.C. Rifflet, F. Millot, Int. J. Thermophys. **26**, 1263 (2005)
5. V.A. Petrov, A.Yu. Vorobyev, in *Collection of Manuscripts of the 17th European Conference on Thermophysical Properties*, ed. by L. Vozar, I. Medved, L. Kubicar, Bratislava, Slovakia, 2005, p. 219
6. F. Millot, B. Glorieux, J.C. Rifflet, AIAA Prog. Astronaut. Aeronaut. **185**, 777 (2000)
7. D.A. Gryvnak, D.E. Burch, J. Opt. Soc. Am. **55**, 625 (1965)
8. L.S. Nelson, N.L. Richardson, K. Keil, S.R. Skaggs, High Temp. Sci. **5**, 138 (1973)
9. H. Abrevaya, P.C. Nordine, J. Am. Ceram. Soc. **71**, 546 (1988)
10. D.O. Nason, C.T. Yen, W.A. Tiller, J. Cryst. Growth **106**, 221 (1990)
11. E.J. Mularz, M.C. Yuen, J. Quant. Spectrosc. Radiat. Transfer **12**, 1553 (1972)
12. N.A. Rubtsov, A.A. Emelyanov, *Experimental Investigation of Optical Properties of Alumina Particle Flow at High Temperatures* (Institut teplofiziki SO AN SSSR, Novosibirsk, 1978) (Preprint No: 25-78)
13. N.A. Rubtsov, A.A. Emelyanov, N.N. Ponomarev, Teplofiz. Vys. Temp. **22**, 294 (1984)
14. N.A. Rubtsov, E.I. Averkov, A.A. Emelyanov, in *Svoistva Teplovogo Izlucheniya Materialov v Kondensirovannom Sostoyanii* (Institut teplofiziki SO AN SSSR, Novosibirsk, 1988), p. 270
15. N.A. Anfimov, G.F. Karabadjak, B.A. Khmelinin, Yu.A. Plastinin, A.V. Rodionov, AIAA Paper 93-2818, in *Presented at 28th Thermophysics Conference* (AIAA, Orlando, 1993)
16. Yu.A. Plastinin, H.Ph. Sipatchev, G.F. Karabadjak, B.A. Khmelinin, A.G. Khlebnikov, Yu.N. Shiskin, AIAA Paper 2000-0735, in *Presented at 38th Aerospace Sciences Meeting & Exhibition* (AIAA, Reno, 2000)
17. C.G. Levi, V. Jayaram, J.J. Valencia, R. Mehrabian, J. Mater. Res. **3**, 969 (1988)
18. M.V. Chase Jr., C.A. Davies, J.R. Downey Jr., D.J. Fryrip, R.A. McDonald, A.H. Syverud, J. Phys. Chem. Ref. Data **14** (Suppl. 1), 158 (1985)
19. J.K.R. Weber, S. Krishnan, C.D. Anderson, P.C. Nordine, J. Am. Ceram. Soc. **78**, 583 (1995)
20. J.K.R. Weber, P.C. Nordine, S. Krishnan, J. Am. Ceram. Soc. **78**, 3067 (1995)
21. T. Noguchi, T. Kozuka, Sol. Energy **10**, 203 (1966)
22. M. Bober, H.U. Karow, K. Muller, High Temp. High Press. **12**, 161 (1980)
23. A.V. Kirillin, A.V. Kostanovskii, V.L. Vinogradov, High Temp. High Press. **19**, 473 (1987)
24. F.A. Akopov, G.E. Val'yano, A.Yu. Vorob'ev, V.N. Mineev, V.A. Petrov, A.P. Chernyshev, G.P. Chernyshov, High Temp. **39**, 244 (2001)
25. A.Yu. Vorob'ev, V.A. Petrov, V.E. Titov, A.P. Chernyshev, High Temp. **45**, 13 (2007)
26. S.V. Krayushkin, A.F. Parfinovich, V.A. Petrov, D.Ya. Svet, A.P. Chernyshev, Teplofiz. Vys. Temp. **24**, 125 (1986)
27. Yu.K. Lingart, V.A. Petrov, N.A. Tikhonova, Teplofiz. Vys. Temp. **20**, 1085 (1982)
28. V.A. Petrov, V.E. Titov, A.Yu. Vorobyev, High Temp. High Press. **31**, 267 (1999)
29. C. Landron, A.K. Soper, T.E. Jenkins, G.N. Greaves, L. Hennet, J.P. Coutures, J. Non-Cryst. Solids **293–295**, 453 (2001)
30. K.S. Bagdasarov, *Visokotemperaturnaya Kristallizatsiya iz Rasplava* (Fizmatlit, Moskva, 2004), pp. 21–28
31. J.-P. Coutures, J.-Cl. Rifflet, P. Florian, D. Massiot, Rev. Int. Hautes Temp. Refract., Fr. **29**, 123 (1994)
32. Y. Waseda, K. Sugiyama, J.M. Toguri, Z. Naturforsch. **50a**, 770 (1995)
33. S. Ansell, S. Krishnan, J.K.R. Weber, J.J. Felten, P.C. Nordine, Phys. Rev. Lett. **78**, 464 (1997)
34. C. Landron, L. Hennet, D. Thiaudiere, Anal. Sci. **17** (Suppl.), i165 (2001)
35. C. Landron, L. Hennet, T.E. Jenkins, G.N. Greaves, J.P. Coutures, A.K. Soper, Phys. Rev. Lett. **86**, 4839 (2001)
36. M.A. San Miguel, J. Fernandes, L.J. Alvares, J.A. Ordiozola, Phys. Rev. B **58**, 2369 (1998)
37. G. Gutierres, A.B. Belonoshko, R. Ahuja, B. Johansson, Phys. Rev. E **61**, 2723 (2000)
38. R. Ahuja, J.M. Osorio-Guillen, J. Souzade Almeida, B. Holm, W.Y. Ching, B. Johansson, J. Phys.: Condens. Matter **16**, 2891 (2004)
39. S. Krishnan, D.L. Price, J. Phys.: Condens. Matter **12**, R145 (2000)
40. V.A. Petrov, A.Y. Vorobyev, A.P. Chernyshev, High Temp. High Press. **34**, 657 (2002)

41. F.A. Akopov, G.E. Val'yano, A.Yu. Vorob'ev, V.N. Mineev, V.A. Petrov, A.P. Chernyshev, G.P. Chernyshev, High Temp. **39**, 244 (2001)
42. V.A. Petrov, A.P. Chernyshev, High Temp. **37**, 58 (1999)
43. A.Yu. Vorob'ev, V.A. Petrov, V.E. Titov, A.P. Chernyshev, Teplofiz. Vys. Temp. **30**, 281 (1982)